OPEN ACCESS

REPORT

The Innovation Life

Ovarian extracellular matrix hydrogel microspheres increase the efficacy of stem cell treatment in premature ovarian insufficiency

Xuemin Liu,[1] Ming Chen,[4] Xiaojie Liang,[2,3] Peixian Cheng,[1] Zeshen Liang,[2,3] Yong Fan,[1,*] and Xuetao Shi[2,3,*]

*Correspondence: yongfan011@gzhmu.edu.cn (Y.F.); shxt@scut.edu.cn (X.S.)

Received: March 12, 2025; Accepted: July 3, 2025; Published Online: July 7, 2025; https://doi.org/10.59717/j.xinn-life.2025.100147

GRAPHICAL ABSTRACT

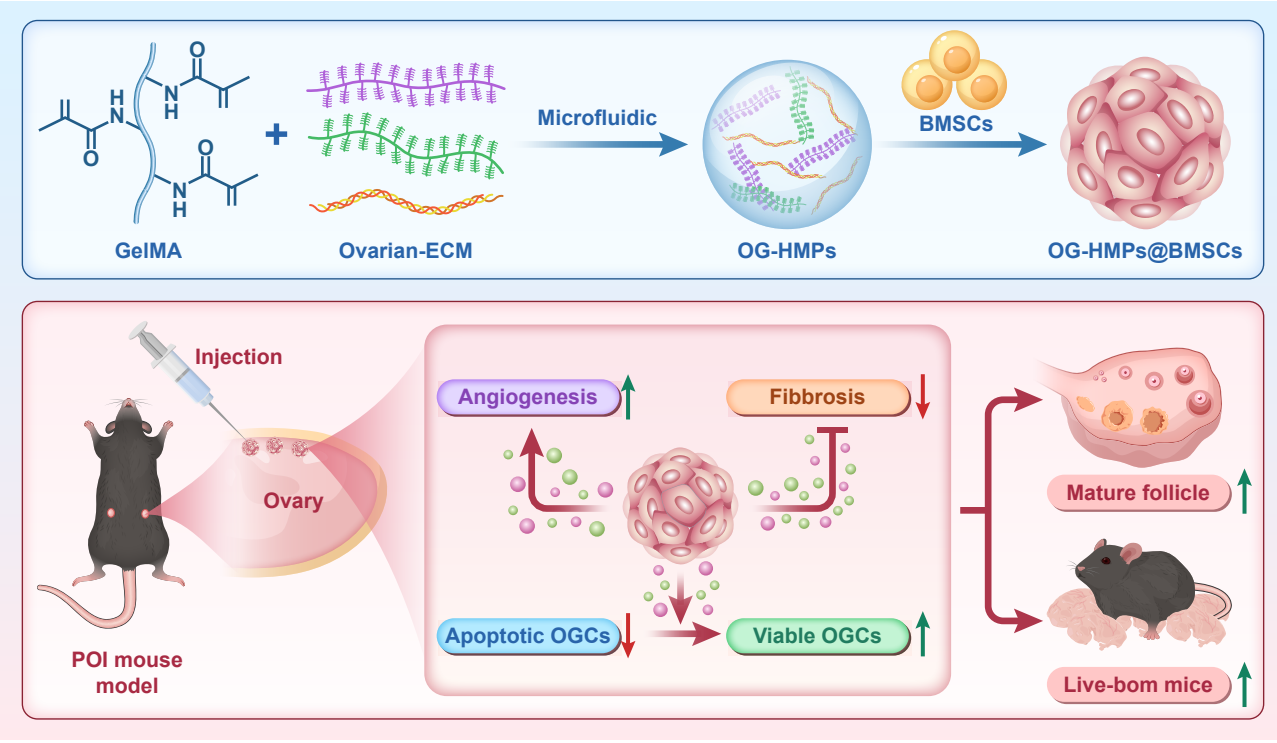

PUBLIC SUMMARY

- Ovarian-ECM hydrogel microspheres serve as an effective carrier for BMSCs delivery.
- OG-HMPs enhance BMSCs proliferation and paracrine effects in vitro.
- OG-HMPs prolong BMSCs retention time in ovaries.
- OG-HMPs@BMSCs restore estrous cycles and reproductive outcomes in POI mice.

REPORT

Ovarian extracellular matrix hydrogel microspheres increase the efficacy of stem cell treatment in premature ovarian insufficiency

Xuemin Liu,[1] Ming Chen,[4] Xiaojie Liang,[2,3] Peixian Cheng,[1] Zeshen Liang,[2,3] Yong Fan,[1,*] and Xuetao Shi[2,3,*]

[1]Department of Obstetrics and Gynecology, Guangdong Provincial Key Laboratory of Major Obstetric Diseases; Guangdong Provincial Clinical Research Center for Obstetrics and Gynecology; Guangdong-Hong Kong-Macao Greater Bay Area Higher Education Joint Laboratory of Maternal-Fetal Medicine; The Third Affiliated Hospital, Guangzhou Medical University, Guangzhou 510150, China

[2]National Engineering Research Centre for Tissue Restoration and Reconstruction and Key Laboratory of Biomedical Engineering of Guangdong Province South China University of Technology Guangzhou 510640, China

[3]Key Laboratory of Biomedical Engineering of Guangdong Province, South China University of Technology, Guangzhou 510006, China

[4]The First Affiliated Hospital of Shenzhen University, Reproductive Medicine Centre, Shenzhen Second People's Hospital, Shenzhen 518035, China

*Correspondence: yongfan011@gzhmu.edu.cn (Y.F.); shxt@scut.edu.cn (X.S.)

Received: March 12, 2025; Accepted: July 3, 2025; Published Online: July 7, 2025; https://doi.org/10.59717/j.xinn-life.2025.100147

Citation: Liu X., Chen M., Liang X., et al. (2025). Ovarian extracellular matrix hydrogel microspheres increase the efficacy of stem cell treatment in premature ovarian insufficiency. *The Innovation Life* **3**:100147.

Premature ovarian insufficiency (POI) affects approximately 1-2% of reproductive-aged women, significantly impacting their reproductive potential and systemic health. Stem cell-based therapy has demonstrated promising therapeutic efficacy in restoring ovarian function through promoting neovascularization, attenuating fibrosis, and suppressing ovarian cell apoptosis. However, conventional cell transplantation approaches are limited by poor cell viability and retention. Here, we developed a novel therapeutic strategy utilizing hydrogel microspheres (OG-HMPs) fabricated from decellularized ovarian extracellular matrix (OECM) and gelatin as delivery vehicles for bone marrow mesenchymal stem cells (BMSCs) to treat POI. OG-HMPs effectively supported BMSCs attachment and proliferation, facilitating the formation of high-density cellular spheroids. The retained ovary-specific bioactive components in OECM recapitulate the native ovarian microenvironment, enhancing cell survival and significantly elevating the expression of angiogenic factors including VEGF and HGF. Moreover, OG-HMPs@BMSCs demonstrate immunomodulatory effects on activated macrophages and cytoprotective properties against chemically-induced granulosa cell apoptosis. In vivo studies using POI mouse models confirmed that OG-HMPs@BMSCs transplantation significantly enhanced BMSCs retention within ovarian tissue and improved both endocrine function, estrous cycle pattern, and reproductive outcomes compared to conventional cell delivery. Collectively, OG-HMPs, exhibiting excellent biocompatibility and biological activity, represent a promising therapeutic platform for POI treatment through enhanced stem cell-mediated tissue regeneration.

INTRODUCTION

Premature ovarian insufficiency (POI), also known as premature ovarian failure, is a common disorder in women characterized by a reduced ovarian reserve and abnormally low estradiol levels, leading to premature loss of ovarian function.[1] The etiology of POI is diverse and includes genetic, immune, iatrogenic, and environmental factors.[2,3] Predominantly, chemotherapeutic agents such as cyclophosphamide, which are commonly used in cancer treatment and autoimmune disease management, can induce premature ovarian insufficiency as a severe adverse effect through direct gonadotoxicity and accelerated follicular depletion.

Currently, hormone replacement therapy (HRT) remains the most common clinical treatment for POI. However, the use of HRT in the treatment of POI remains controversial, as HRT is considered unsafe for women with a history of breast or ovarian cancer and is unable to reduce the impact of autoimmune ovarian damage.[4] Emerging therapeutic approaches under investigation include in-vitro follicle culture, immunomodulatory therapies, and stem cell-based interventions, which show promise in restoring ovarian function and fertility but remain experimental.[5] Advances in understanding the immunological and genetic underpinnings of POI have spurred research into targeted immunotherapies and regenerative medicine, offering new avenues for treatment beyond hormone replacement. Additionally, fertility preservation strategies, such as ovarian tissue cryopreservation prior to gonadotoxic treatments, are increasingly integrated into clinical practice to mitigate iatrogenic POI.[6]

Mesenchymal stem cells (MSCs), particularly those derived from adipose tissue, bone marrow, the umbilical cord, and the placenta, exhibit remarkable multipotency and proliferative capacity.[7] In POI animal models, MSCs transplantation can restore the ovarian reserve by inducing the secretion of various cytokines, exerting anti-inflammatory and immunomodulatory effects, and regulating DNA repair processes, promoting recovery of ovarian function.[8] These mechanisms collectively promote angiogenesis, suppress tissue fibrosis, and protect ovarian granulosa cells (OGCs) from apoptosis, thereby enhancing ovarian microenvironment reconstruction.[9,10] Among these, bone marrow mesenchymal stem cells (BMSCs) possess distinct advantages, including easy accessibility and low immunogenicity, enabling potential allogeneic transplantation.[11,12] Previous studies have shown that BMSCs play an effective role in improving ovarian function to treat ovarian failure and infertility.[13,14] Traditional stem cell delivery methods such as intravenous injection and direct tissue injection are limited by poor cell survival and limited retention efficiency, which compromises their therapeutic efficacy. Intravenous injection faces challenges of substantial cell entrapment in non-target organs including lungs and liver,[5] while direct tissue injection often results in low post-implantation cell viability due to lack of appropriate microenvironmental support.[16] Although hydrogel encapsulation has been extensively investigated to improve stem cell delivery, existing hydrogel systems still have limitations in providing ovary-like physiological microenvironments, particularly in supporting follicular development.[17]

To overcome these limitations, this study proposes an innovative stem cell delivery strategy that involves the use of hydrogel microspheres (OG-HMPs) synthesized from ovarian tissue-derived extracellular matrix (OECM) and gelatin as carriers for BMSCs. First, extracellular matrix (ECM) materials possess excellent biocompatibility, not only supporting cell growth but also regulating cell adhesion and proliferation; inducing cell differentiation; modulating immune cell functions; and promoting damaged tissue repair.[18–20] Moreover, OECM mimic the natural ovarian microenvironment, providing an ideal survival and functional environment for transplanted cells.[21,22] Previous studies have indicated that ovarian-derived OECM scaffolds can support the growth of ovarian mesenchymal cells and ovarian tissue, contributing to the restoration of ovarian function and demonstrating great potential in the construction of experimental artificial ovaries.[23] Furthermore, stem cells delivered by hydrogel microspheres (HMPs) showed prolonged retention in target tissues, increased survival rates, and improved functional efficacy, thereby increasing their therapeutic potential.[24,25]

This study investigated the regulatory effects of OG-HMPs on BMSCs and evaluated their therapeutic potential in POI treatment via OG-HMPs@BMSCs delivery system. We assessed the influence of OG-HMPs on BMSC viability, proliferation, and gene expression *in vitro*. The OG-HMPs exhibited favorable biocompatibility, supporting BMSCs proliferation while enhancing the expression of multiple growth factors. In co-culture systems with macrophages and OGCs, OG-HMPs@BMSCs effectively attenuated inflammatory responses in macrophages and protected OGCs against chemically induced apoptosis. In

a POI mouse model, compared to conventional cell injection, OG-HMPs significantly enhanced the retention of transplanted BMSCs within ovarian tissue and improved ovarian endocrine function and fertility outcomes. These findings suggest that OG-HMPs represent a promising platform for POI treatment through enhanced stem cell-mediated tissue regeneration.

MATERIALS AND METHODS

Materials

Sodium dodecyl sulfate (SDS), gelatin (type A, from porcine skin), and the photoinitiator lithium phenyl-2,4,6-trimethylbenzoylphosphinate (LAP) were purchased from Sigma-Aldrich. GelMA was synthesized as previously described.[26] Liquid paraffin and Span 80 were obtained from Macklin. Dulbecco's modified Eagle's medium (DMEM), fetal bovine serum (FBS), and antibiotics were purchased from Gibco, USA. A Cell Counting Kit-8 (CCK-8) was obtained from Dojindo. A live/dead cell staining kit was purchased from Invitrogen. Antibodies against α-SMA and VEGF were obtained from Abcam. Antibodies against INHBA and AMH were obtained from ABclonal. Antibodies against Ki67 were obtained from Affinity.

Synthesis and characterization of OG-HMPs

The OECM was extracted from juvenile porcine ovaries (2 months old) following the previously established protocols.[27] Briefly, after removing all antral follicles and corpora lutea, the ovaries were rinsed with deionized water and then sliced into tissue fragments of 1 cm^3. In order to eliminate intracellular components, the ovarian tissue blocks were washed with a 1% sodium dodecyl sulfate (SDS) solution while stirring at 400 rpm/min for 18 hours. The SDS solution was changed every 6 hours. The ovarian tissues were rinsed three times with PBS containing antibiotics (100 U/mL penicillin-streptomycin) after being treated with SDS, for a total of 24 hours. Following washing, the flesh-colored ovarian tissue turned white, signifying the decellularized state. 0.1% peracetic acid in 4% ethanol was used to sterilize the decellularized ovarian tissue.

The decellularized tissue was subsequently lyophilized and digested with 1 mg/mL pepsin (P7000, Sigma, USA) to obtain the OECM solution. The quality of decellularization was verified by quantifying residual DNA content (Quant-iT™ PicoGreen™ dsDNA Reagent and Kit, Invitrogen, USA). The biochemical composition was characterized by measuring collagen content (Sircol™ Soluble Collagen Assay, Biocolor Ltd., UK) and sulfated glycosaminoglycan (GAG) content via DMMB assay. OECM was then modified with methacrylate groups through reaction with methacrylic anhydride under controlled pH conditions, and the successful modification was confirmed by 1H NMR spectroscopy (Bruker AVIII500 M, Switzerland). This OECM solution was then functionalized with methacryloyl groups to create methacryloyl OECM (OECMMA) for subsequent hydrogel formation. Detailed information is provided in the supplementary materials.

A hydrogel prepolymer solution comprising 10% (w/v) Gelatin methacryloyl (GelMA), 1% (w/v) OECMMA, and 0.25% (w/v) photoinitiator lithium phenyl-2,4,6-trimethylbenzoylphosphinate (LAP) was subsequently prepared. For the control group, OECMMA was omitted from the prepolymer solution. Using microfluidic chips, the hydrogel prepolymer solution (aqueous phase) served as the inner phase, whereas liquid paraffin containing 0.5 wt% Span 80 (oil phase) functioned as the outer phase. The prepared solutions remained stable for several weeks. Microfluidic droplet generation was performed with flow rates of 24 μL/min (inner phase) and 60 μL/min (outer phase). The extruded microdroplets were exposed to UV light (405 nm, 20 mW/cm^2) for 2 min, followed by centrifugation and multiple PBS washes to collect HMPs (OG-HMPs and G-HMPs). The surface morphology of the lyophilized HMPs was examined by scanning electron microscopy (SEM) (Merlin Carl Zeiss AG, Germany). In vitro degradation studies of G-HMPs and OG-HMPs were conducted in PBS (pH 7.4) containing type I collagenase (1 U/mL) supplemented with 0.02% sodium azide to prevent microbial contamination.

In vitro cytocompatibility and functional assessment

To evaluate the in vitro cytocompatibility of OG-HMPs, mouse BMSCs (passages 3-5, American Type Culture Collection ATCC) were seeded onto the microsphere surface. Briefly, 1 mL of densely packed OG-HMP microspheres (approximately 8×10^4 particles) was obtained through centrifugation (1100 rpm, 5 min) and subsequently combined with 5 mL of BMSCs suspension (2×10^5 cells/mL in complete DMEM) to achieve a final cell-to-microsphere ratio of 1×10^6 cells per 1 mL of densely packed microspheres. The suspension was subjected to gentle agitation (60 rpm, 5 min) to facilitate homogeneous cell distribution, followed by sedimentation to concentrate the cell-microsphere complexes. Following a 30-minute incubation period at 37°C in a humidified atmosphere containing 5% CO_2 to promote initial cellular adhesion, the suspension was carefully homogenized and aliquoted into 24-well ultra-low attachment plates (0.5 mL per well) with supplementation of an additional 0.5 mL of culture medium. Medium replacement was performed every 3 days.

Cell viability and proliferation were assessed via a Cell Counting Kit-8 (CCK-8) assay at days 1, 4, and 7 postseeding. Briefly, CCK-8 solution was added to the culture medium, and the absorbance was measured after 45 min of incubation. Concurrently, the cell density, morphology, and adhesion on the microsphere surface were visualized via Live/Dead fluorescent staining in conjunction with confocal laser scanning microscopy. Furthermore, after 5 days of coculture, the BMSCs-loaded microspheres were collected via centrifugation for immunofluorescence staining of Ki67 (a proliferation marker) and VEGF (vascular endothelial growth factor). Additionally, real-time quantitative polymerase chain reaction (RT-qPCR) was performed to quantify the mRNA expression levels of VEGF, hepatocyte growth factor (HGF), and insulin-like growth factor 1 (IGF-1) in the BMSCs. The cell supernatants were analyzed for VEGF and HGF levels using the Mouse VEGF ELISA Kit (EK283/2-02, MultiSciences, China) and the Mouse HGF ELISA Kit (EK2H01-AW1, MultiSciences, China) according to the manufacturers' protocols.

Modulation of macrophage inflammation

To investigate the immunomodulatory effects of OG-HMPs@BMSCs on inflammatory macrophages, a coculture system was established. Macrophages (RAW264.7 murine macrophage cell line) (2×10^5 cells/well) were first induced into an inflammatory state by treatment with lipopolysaccharide (LPS, 200 ng/mL) and interferon-gamma (IFN-γ, 2.5 ng/mL) for 12 hours. Subsequently, OG-HMPs@BMSCs or an equivalent number of BMSCs (2×10^5 cells/well) were cocultured with the induced inflammatory macrophages via a Transwell system for 24 or 48 hours. BMSCs or OG-HMPs@BMSCs were placed in the upper chamber of the Transwell, while activated macrophages were located in the lower chamber.

The levels of inflammatory cytokines (IL-1β, IL-6, TNF-α, and IL-10) in the culture supernatant were quantified via ELISA. To assess macrophage polarization, the RAW264.7 cell suspension was analyzed via flow cytometry to determine the M1/M2 macrophage ratio. M1 macrophages were identified as $F4/80^+$ $CD11b^+$ $iNOS^+$ macrophages, whereas M2 macrophages were identified as $F4/80^+$ $CD11b^+$ $Arg1^+$ macrophages. Intracellular NO levels were measured using a DAF-FM DA fluorescent probe (Beyotime Biotechnology, S0019S, China) following the manufacturer's protocol. Briefly, RAW264.7 cells were incubated with 5 μM DAF-FM DA in serum-free medium for 30 min at 37°C in the dark. After the samples were washed three times with PBS, the fluorescence intensity was analyzed by confocal microscopy (Ex/Em: 495/515 nm, Zeiss LSM980, Germany).

In vitro apoptosis levels of OGCs

Mouse ovarian granulosa cells (OGCs) (Passage 1, derived from female C57BL/6 mice) were obtained from Pricella Co., China. OGCs were cultured in specialized granulosa cell medium (Pricella Co., China) supplemented with 15% fetal bovine serum (FBS), 100 U/mL penicillin, 100 μg/mL streptomycin, 10 ng/mL epidermal growth factor (EGF), and 5 μg/mL insulin. Cells were maintained at 37°C in a humidified atmosphere containing 5% CO_2 and passaged at 80% confluence approximately every 3 days using 0.25% trypsin-EDTA.

For apoptosis and proliferation analysis, OGCs were seeded in 6-well plates at a density of 2×10^5 cells/well and cultured for 24 hours to allow attachment. Subsequently, cells were exposed to 5 μM phosphoramide mustard to induce cellular damage and simulate POI conditions *in vitro*. Phosphoramide mustard, the active metabolite of cyclophosphamide *in vivo*, was selected for *in vitro* experiments due to its direct cytotoxic effects on ovarian cells and its established role in chemotherapy-induced ovarian failure. Following phos-

phoramide mustard treatment, damaged OGCs were co-cultured with either BMSCs or OG-HMPs@BMSCs (2×10^5 cells/well) using a Transwell system (Polycarbonate film, 0.4 μm pore size, Corning). Then, OGCs were stained with Annexin V and propidium iodide (PI) (Beyotime, China) according to the manufacturer's instructions. The percentage of apoptotic cells was quantified via flow cytometry.

POI model establishment and assessment

All animal experiments described in this study were approved by the Institute of Animal Care and Use Committee of South China University of Technology. All animal experiments abided by the Animal Research: Reporting of *In Vivo* Experiments (ARRIVE) guidelines. A chemically induced POI mouse model was established in 8- to 10-week-old female C57BL/6 mice weighing 20-25 g. POI model mice were intraperitoneally injected with cyclophosphamide at a dose of 40 mg/kg per day for 8 days, and then with cyclophosphamide at a dose of 20 mg/kg per day for seven consecutive days.[28] The successful establishment of the POI model was evaluated through multiple parameters. The serum levels of estradiol (E2), follicle-stimulating hormone (FSH), and anti-Müllerian hormone (AMH) were quantified via ELISA. The estrous cycle was monitored daily through vaginal cytology for 14 consecutive days. Ovarian histology was assessed via Masson trichrome staining to evaluate follicle numbers and ovarian tissue structure, respectively.

BMSCs transplantation and *in vivo* tracking

POI model mice were randomly assigned to three groups (n = 12): the untreated POI group (injected with 50 μL of saline), the mouse BMSCs group (injected with 50 μL of a cell suspension containing 6×10^5 mouse BMSCs, and the OG-HMPs@BMSCs group (injected with 50 μL of OG-HMPs loaded with 6×10^5 mouse BMSCs). Additionally, a Normal group (n=12, healthy mice without treatment) was set as a positive control. The mice were maintained under standard laboratory conditions with free access to food and water throughout the experiment.

To evaluate the retention time and distribution of BMSCs *in vivo*, we designed a cell tracking experiment, with three mice per group. The BMSCs were labeled with the lipophilic Far-red fluorescent dye, 1,1'-dioctadecyl-3,3,3',3'-tetramethylindodicarbocyanine (DiD). For the direct injection group, 5×10^6 labeled BMSCs were injected under the ovarian capsule of each mouse. The microsphere delivery group received an equivalent number of BMSCs adhered onto OG-HMPs and then suspended in solution. Fluorescence imaging was performed via an IVIS Spectrum *in vivo* imaging system on days 0, 1, 3, 7, and 14 post-transplantation, using an excitation wavelength of 640 nm and an emission wavelength of 680 nm.

Assessment of ovarian function

Serum hormone levels and estrous cycle monitoring. On days 14 and 28 posttreatment initiation, blood samples were collected from the mice. Serum was obtained by centrifugation (4000 rpm, 10 minutes) and analyzed for E2, FSH, and AMH concentrations using ELISA kits (E2: CEA461Ge, Cloud-Clone Corp. (China, Wuhan); FSH: CEA830Mu, Cloud-Clone Corp. (China, Wuhan); AMH: CEA228Mu, Cloud-Clone Corp. (China, Wuhan) according to the manufacturers' instructions. All samples were measured in triplicate, and the average values were used for statistical analysis.

Histological and immunostaining analysis

From day 14 to day 28 post-treatment, vaginal secretions were collected daily for 14 consecutive days. Vaginal smears were obtained via a moistened cotton swab, spread evenly on glass slides, air-dried, and stained with Giemsa dye. On day 28 post-treatment, a subset of the mice was euthanized, and ovarian and uterine tissues were collected. First, ovarian wet weight and mouse body weight were precisely measured to calculate the ovarian index (ovarian wet weight/body weight). Several ovarian tissues were subsequently processed for routine histological examination; they were fixed in 4% paraformaldehyde for 24 hours, dehydrated through a graded ethanol series, cleared in xylene, and embedded in paraffin. Using a microtome, 5 μm thick serial sections were prepared and stained with Masson's trichrome. Follicles at different developmental stages, including primordial, primary, and secondary follicles, were counted.

To comprehensively evaluate the effects of different treatments on ovarian tissue in POI model mice, we performed a series of immunohistochemistry and immunofluorescence staining analyses on 4 μm thick ovarian tissue sections. First, VEGFA and α-SMA antibodies were used to label blood vessels and fibrous tissue, respectively. Multiplex immunofluorescence staining were subsequently conducted in two groups: (1) DAPI (cell nuclei), AMH (ovarian reserve), and follicle-stimulating hormone receptor (FSHR) (ovarian function) and (2) DAPI (cell nuclei), Ki67 (cell proliferation marker), and INHBA (follicle development-related marker). We also performed immunohistochemical staining for Caspase 3 to assess apoptosis.

Images were captured via fluorescence or confocal microscopy under standardized exposure conditions. Immunofluorescence images were analyzed through ImageJ with individual channel processing. Five random regions of interest (ROIs) per sample were quantified for mean fluorescence intensity (MFI), with nuclear MFI serving as an internal normalization factor to account for cell density variations. The relative fluorescence intensity was calculated as: Marker protein MFI / Nuclear MFI. Detailed information of antibody is provided in the supplementary materials.

Fertility assessment

Following 28 days of treatment, mating trials were performed to evaluate reproductive function. The experimental cohorts consisted of the POI group (n = 5), BMSCs-treated group (n = 4), OG-HMPs@BMSCs group (n = 4), and Normal group (n = 5). To eliminate potential sex-related confounding factors, two female mice from distinct experimental groups were paired with a single 8-10-week-old male mouse for a 7-day cohabitation period. Pregnancy outcomes were monitored, and birth rates were assessed 20 days post mating by recording delivery dates and live pup numbers per dam.

Statistical analysis

Data are presented as means ± SD (n ≥ 3). One-way analysis of variance (ANOVA) was performed for differences between multiple groups. $p < 0.05$ was considered to indicate statistical significance. * $p < 0.05$, ** $p < 0.01$, *** $p < 0.001$ and **** $p < 0.0001$..

RESULTS AND DISCUSSIONS

Synthesis and characterization of OG-HMPs

The intrinsic properties of gelatin, including its safe biodegradability and strong cell adhesion capacity, establish it as a prime candidate for hydrogel matrix applications. GelMA, a photocrosslinkable derivative of gelatin, was selected as a primary component for our hydrogel microspheres. In our previous study, GelMA maintains the excellent biocompatibility and cell adhesion properties of natural gelatin while offering tunable mechanical properties through controlled photopolymerization.[26,29] The presence of cell-binding motifs (such as RGD sequences) in GelMA provides excellent support for cell attachment and proliferation.[30] GelMA was synthesized via an amidation reaction between amino groups on gelatin molecular chains and methacrylic anhydride. Nuclear magnetic resonance (NMR) spectroscopy revealed double bond grafting rates of 86% for GelMA (Figure S1A). Decellularization of native ovarian tissue was performed, followed by pepsin digestion to yield an ovarian extracellular matrix (OECM) (Figure 1A). The process of ovarian tissue decellularization effectively removed the nucleus while preserving the matrix framework and essential extracellular matrix proteins of ovarian tissue (Figure S2). The periodic acid-schiff (PAS) staining images showed that decellularized ovarian tissue maintained substantial ECM components despite cellular removal (Figure S3). PAS-positive staining (magenta/purple-red) was observed throughout the decellularized scaffolds, indicating successful preservation of polysaccharides and glycoproteins essential for maintaining ECM structural integrity and bioactivity. Proteomic analysis of three parallel OECM samples revealed 31 major identical proteins, indicating consistent protein composition due to effective decellularization (Figure S4A). The OECM components were composed of collagen (30.8%), glycoproteins (19.2%), ECM-affiliated proteins (23.1%), cell-secreted factors (11.25%), and proteoglycans (7.7%) (Figure S4B). The top ten proteins were highly reproducible across samples (Figure S4C). COL1A2 and COL1A1 were the most abundant proteins of OECM. Studies have demonstrated that COL1 expression correlates with MSCs adhesion and promotes tissue repair by guiding

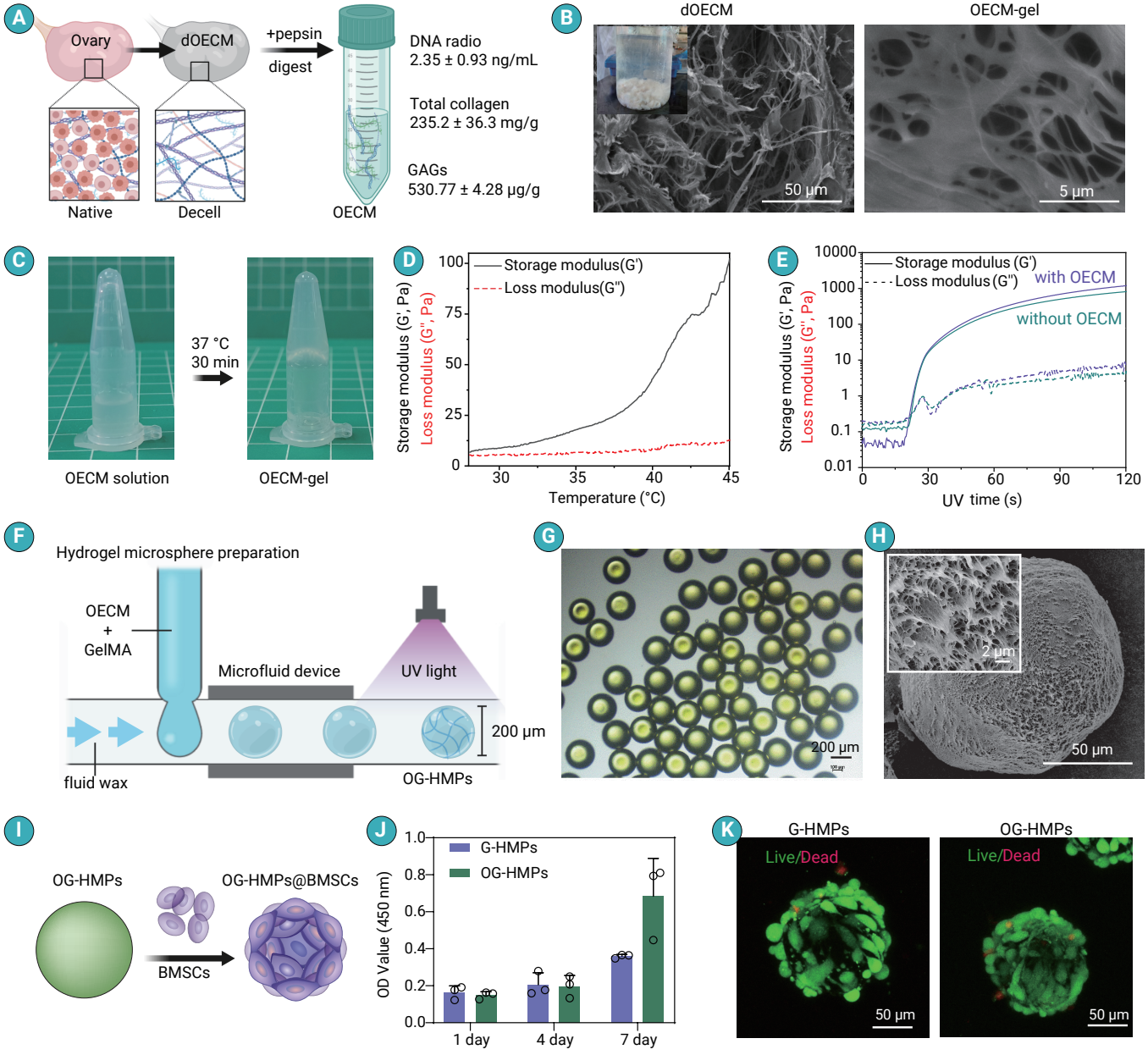

Figure 1. Characterization and biocompatibility evaluation of hydrogel microspheres (OG-HMPs) (A) Schematic illustration of the decellularization process for OECM, created in BioRender (Liu, X. (2025) https://BioRender.com/e74y943). (B) SEM images of decellularized ovarian tissue and the resulting OECM hydrogel. Scale bar: 10 μm. (C) Macroscopic image of OECM gel formation after incubation in 2% OECM solution at 37°C for 30 minutes. (D) Dynamic modulus (storage modulus (G') and loss modulus (G")) of the OECM solution (2%) as a function of temperature. (E) The real-time variation in the G' and G" values of the 10% GelMA with or without OECM during radical polymerization was measured by oscillating-frequency scanning (10 rad s^{-1}; 1% strain) under 20 mW cm^{-2} ultraviolet light (405 nm). (F) Schematic diagram of the microfluidic process for HMPs preparation. (G) Size distribution of OG-HMPs. Scale bar: 200 μm. (H) SEM images of OG-HMPs: surface morphology at high magnification (inset, scale bar: 5 μm) and overall spherical structure (scale bar: 50 μm). (I) Schematic illustration of BMSCs loaded onto HMPs *in vitro*. (J) CCK-8 assay showing BMSCs proliferation levels at 1, 4, and 7 days (n=3). (K) Live/dead fluorescence staining images (live cells are green, dead cells are red). Scale bar: 50 μm.

MSCs migration to injury sites.[31] Additionally, COL5A2 is upregulated during follicle development and may be involved in the remodeling of the follicle wall and follicle maturation.[32,33]

The extent of decellularization, quantified by residual DNA content, significantly influences host response to ECM scaffolds, with insufficient processing leading to adverse immune reactions.[34] The decellularized OECM exhibited minimal residual DNA content (2.5 ± 0.93 ng/mg), far below the recommended criterion (50 ng/mg) for biocompatible tissue scaffolds, while maintaining high levels of total collagen (235.2 ± 36.3 mg/g) and glycosaminoglycan (GAG) (530.77 ± 4.28 μg/g). SEM images revealed that decellularized ovarian tissue (dOECM) maintained fibrous structures, while the OECM-gel formed through sol-gel transition (37°C, 30 min) exhibited an interconnected porous network (Figures 1B-C). The storage modulus (G') and loss modulus (G") of different hydrogels were analyzed via rheological characterization. As the temperature increased from 30°C to 45°C, G' significantly increased, indicating increased elasticity, which led to the formation of a hydrogel with 2% OECM (Figure 1D).

To crosslink OECM with GelMA, we grafted carbon-carbon double bonds onto OECM by reacting it with methacrylic anhydride to obtain OECMMA (Figure S1B). The hydrogels (with or without OECMMA) exhibited solid-like elastic behavior (G' >> G") after UV irradiation (405 nm) for 120 s (Figure 1E), with a storage modulus approaching 1000 Pa. The addition of 1% OECMMA to 10% GelMA had a minimal effect on the mechanical properties of the hydrogel (Figure 1E). Hydrogel microspheres were fabricated via microfluidic

technology. The aqueous phase, consisting of 1% OECM, 10% GelMA, and 0.25% LAP (photoinitiator), was emulsified in an oil phase (liquid paraffin with 5% Span 80) to form microspheres, which were subsequently crosslinked under UV light (405 nm, 20 mW) for 2 minutes (Figure 1F). The resulting hydrogel microspheres (OG-HMPs) exhibited a uniform size distribution with an average diameter of 224.7 ± 13.5 μm (Figure 1G), enabling efficient injectable delivery into ovarian tissue. In morphological characterization, SEM imaging revealed the porous structure of the OG-HMPs (Figure 1H). The degradation kinetics exhibited a biphasic pattern: an initial rapid phase over the first 2 days, followed by a slower degradation rate (Figure S5). G-HMPs and OG-HMPs fully degraded by day 18 and day 21, respectively. The addition of OECM most likely altered the hydrogel crosslinking density, which accounts for the observed discrepancies in degradation rates.

Then, we evaluated BMSCs growth on different HMPs (Figure 1I). CCK-8 assays revealed comparable BMSCs proliferation between OG-HMPs and GelMA hydrogel microspheres without OECM (G-HMPs), with significantly increased proliferative activity in OG-HMPs on day 7 (Figure 1J). Live/dead staining revealed high cell viability on both the OG-HMPs and the G-HMPs, indicating excellent biocompatibility and support for cell survival (Figure 1K & S6). BMSCs were seeded on OG-HMPs for 3 days and transferred to culture dishes conducive to BMSCs adhesion and migration, high cell viability and outward cell spreading, resulting in the formation of proliferation zones after 1, 2, and 3 days of *in vitro* culture (Figure S7). These results confirm the excellent biocompatibility, cell proliferation-promoting capacity, and cell adhesion-supporting ability of OG-HMPs for BMSCs delivery.

OG-HMPs maintain BMSCs stemness and enhance paracrine function

To investigate the regulatory effects of OECM components on mouse BMSCs growth and function, we compared cells cultured on OG-HMPs with those cultured on G-HMPs. The results showed that after 3 and 6 days of culture, the expression of VEGF in BMSCs cultured on OG-HMPs was significantly higher than that in BMSCscultured on G-HMPs (Figure 2A). Quantitative fluorescence analysis revealed that the percentage of the VEGF-positive area in the OG-HMPs group was significantly greater than that in the G-HMPs group (Figure 2B). These findings suggest that, in comparison with G-HMPs, OG-HMPs can more effectively upregulate the expression of VEGF in BMSCs, potentially offering a more conducive microenvironment for angiogenesis. Moreover, cell proliferation was evaluated through Ki67 immunofluorescence staining (Figure 2C). On day 3, the percentage of Ki67-positive cells in the OG-HMPs group reached 54.3 ± 9.0%, whereas it reached 38.0 ± 5.3% in the G-HMPs group. After 6 days of culture, the percentage of Ki67-positive cells in the G-HMPs group sharply decreased to 7.3±2.5%, whereas that in the OG-HMPs group remained stable at 21.7 ± 3.8% (Figure 2D). These findings suggest that OG-HMPs are more conducive to maintaining BMSCs proliferative activity, especially during cell growth.

To further verify the expression profiles of the growth factors, quantitative reverse transcription polymerase chain reaction (RT-qPCR) analysis was performed (Figure 2F). VEGF expression was significantly upregulated 7.7-fold and 3.4-fold in the OG-HMP and G-HMP groups compared with the control group (BMSCs grown on a cell culture plate). Notably, VEGF mRNA expression in the OG-HMP group was 2.3 times greater than that in the G-HMP group. Similarly, BMSCs cultured on OG-HMPs and G-HMPs presented increased HGF expression (3.5-fold and 2.8-fold greater than that in the control group, respectively). Although HGF expression was slightly elevated in the OG-HMP group compared with the G-HMP group, this difference was not statistically significant. The IGF-1 expression levels remained comparable across all three groups. Consistent with the gene expression analysis, the results of ELISA showed that the concentration of VEGF in OG-HMPs group (437.9 ± 66.5 pg/mL) was significantly higher than that in G-HMPs group (293.1 ± 23.6 pg/mL) and control group (about 222.4 ± 46.5 pg/mL) (Figure 2E) . Similarly, the level of HGF also showed an upward trend, OG-HMPs group showed the highest expression level, and there were significant differences with the control group and G-HMPs Group. The enhanced secretion of VEGF and HGF plays an important role in promoting neovascularization, anti-apoptotic, and anti-fibrotic effects in MSCs-based therapy.[35,36] OG-HMPs showed superior performance compared to G-HMPs, demonstrating the significance of OECM in maintaining and enhancing cell function. This superiority could be due to the biological active components retained by OECM such as collagen and glycosaminoglycan. These findings provide strong experimental evidence that OG-HMPs serve as an advantageous platform for stem cell delivery *in vivo*, particularly in cell therapy applications.

OG-HMPs@BMSCs had enhanced immunomodulatory effects and increased the survival rate of damaged OGCs

Stem cell therapy usually prevents and restores fertility damage by affecting the stromal microenvironment of the reproductive organs, including suppressing the inflammatory responses of macrophages and reducing germ cell apoptosis.[37] To investigate the regulatory effects of OG-HMPs@BMSCs on macrophage phenotypic transformation, RAW264.7 cells were stimulated with lipopolysaccharide (LPS, 200 ng/mL) and interferon-gamma (IFN-γ, 2.5 ng/mL) for 12 hours. The expression of various inflammatory factors (IL-6 and TNF-α) in macrophages increased significantly, confirming macrophage activation (Figure S8). Meanwhile, IL-10, which is regarded as an anti-inflammatory factor, was also upregulated, possibly because it was in the initial stage of inflammatory activation, due to the feedback regulatory mechanism of the inflammatory response[38] (Figure S8). Subsequently, BMSCs, G-HMPs@BMSCs, and OG-HMPs@BMSCs were separately co-cultured with activated macrophages, and the secretion levels of inflammatory mediators in macrophage culture supernatants were evaluated by ELISA at 24 and 48 hours post-treatment (Figures S9A & 3A). Compared to the control group, all treatment groups with BMSCs significantly reduced TNF-α secretion levels, with no significant differences between these three groups, indicating that BMSCs are key to suppressing TNF-α secretion. Both G-HMPs@BMSCs and OG-HMPs@BMSCs groups showed significantly lower IL-6 levels compared to the BMSCs alone group (Figure 3A). Furthermore, the expression levels of the anti-inflammatory cytokine IL-10 showed a progressive increase from BMSCs, G-HMPs@BMSCs, to OG-HMPs@BMSCs groups (Figures S9A & 3A), indicating that OECM further enhances the anti-inflammatory effects of BMSCs. The expression levels of the anti-inflammatory cytokine IL-10 exhibited a gradual elevation pattern and reaching the highest level in the OG-HMPs@BMSCs group. This trend suggests that the OECM modification effectively potentiates the anti-inflammatory capacity of BMSCs through functional enhancement.

To further validate these findings, we analyzed the proportions of M1 macrophages ($F4/80^+$ $CD11b^+$ $iNOS^+$) and M2 ($F4/80^+$ $CD11b^+$ Arg^+) macrophages in treated RAW264.7 cells using flow cytometry (Figure S9B). Compared to the control group, all BMSCs-containing treatment groups showed significantly increased M2 macrophage proportions and decreased M1 macrophage proportions (Figure 3B & S9B). Notably, the OG-HMPs@BMSCs group achieved the highest M2 macrophage proportion at 21.83±1.89%, significantly higher than both the BMSCs group (16.76±2.49%) and G-HMPs@BMSCs group (17.27 ± 1.75%) (Figure 3B). Additionally, nitric oxide (NO) production was monitored using a red fluorescent NO probe. The stimulation of LPS and IFN-γ markedly elevated NO production in RAW264.7 cells compared to untreated controls. While both BMSCs alone and G-HMPs@BMSCs treatments significantly reduced NO production, OG-HMPs@BMSCs demonstrated the most potent inhibitory effect (Figure 3C). Collectively, these results confirm the enhanced immunomodulatory capacity of OG-HMPs@BMSCs in regulating macrophage-mediated inflammatory responses.

To evaluate the protective effects against chemotherapy-induced ovarian damage, primary mouse OGCs were treated with phosphoramide mustard (5 μM), the active metabolite of cyclophosphamide. Phosphoramide mustard was specifically selected for *in vitro* experiments as it exerts direct cytotoxic effects on ovarian cells and plays a crucial role in chemotherapy-induced ovarian failure. Following this damage induction, OGCs were co-cultured with BMSCs alone, G-HMPs@BMSCs, or OG-HMPs@BMSCs in a transwell system for 48 hours. This experimental design allowed us to assess the paracrine effects of different delivery systems without direct cell-cell contact. BMSCs exert their protective effects via paracrine mechanisms, secreting a variety of growth factors like VEGF, HGF and 1-IGF and achieving their anti-apoptotic effects.[39] By comparing the protective efficacy of BMSCs delivered

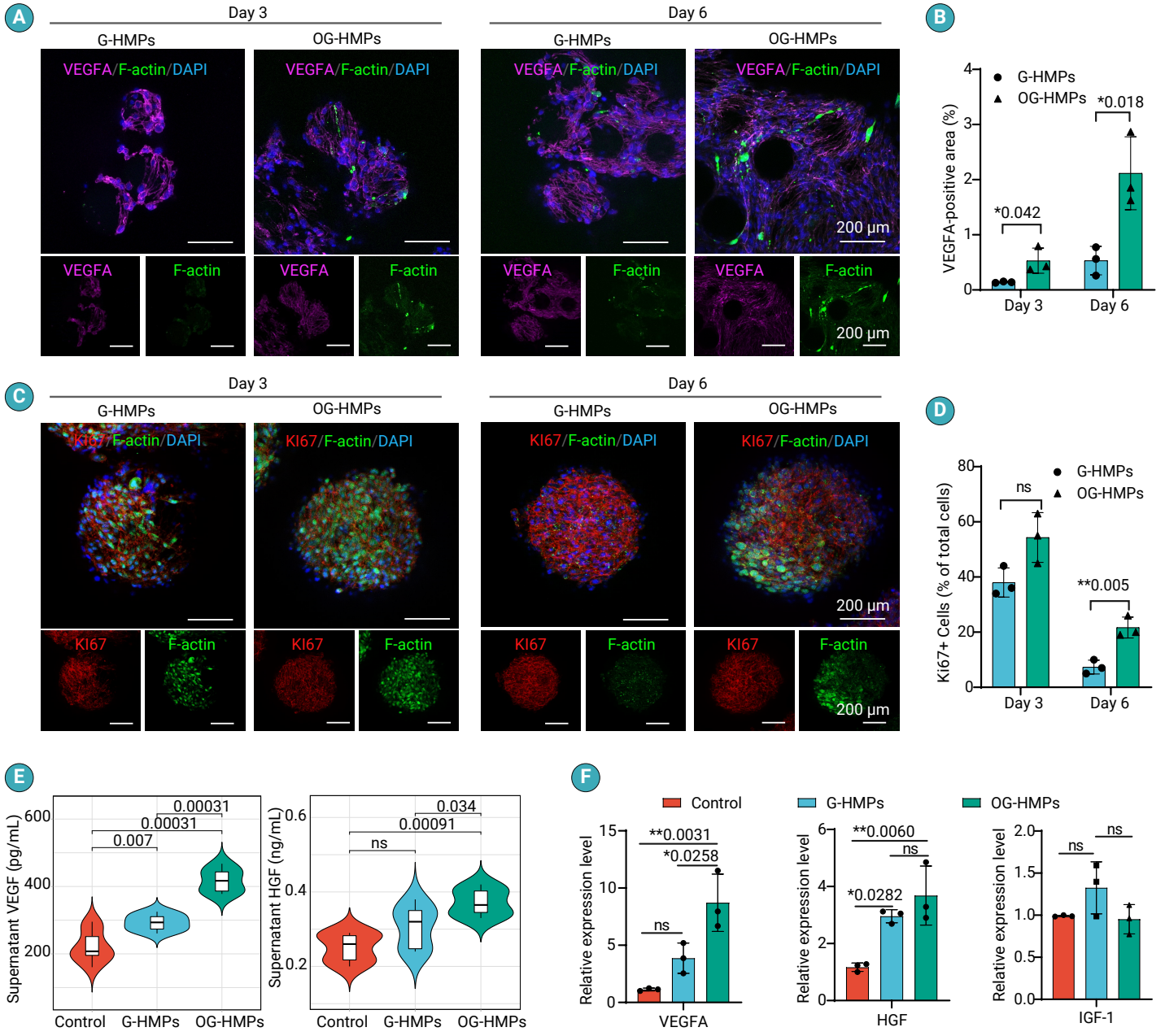

Figure 2. Growth factor expression and proliferation of BMSCs (A&C) Immunofluorescence staining of VEGF-positive cells (A) and Ki67-positive cells (C) (green) in the G-HMP and OG-HMP groups. Nuclei were counterstained with DAPI (blue). Scale bar = 200 μm. (B) Statistical analysis of The percentage of VEGF-positive fluorescent area. (D) The percentage of Ki67 - positive cells relative to the total number of cells. (E) The concentrations of VEGF and HGF in Control, G-HMPs and OG-HMPs groups were quantified by ELISA. Statistical analysis was performed using Student's t-test in R package v.4.4.2. (F) RT-qPCR analysis of the mRNA expression levels of growth factors (VEGF, HGF, and IGF-1) in BMSCs. The data are presented as the means ± standard deviations (SD) (n = 3). Statistical analysis was performed using one-way analysis of variance (ANOVA) followed by Tukey's multiple comparison test. * $p < 0.05$, ** $p < 0.01$.

via different ways, we could evaluate whether OG-HMPs enhanced the paracrine function of BMSCs in protecting damaged ovarian cells. Flow cytometry analysis revealed that while the control group showed an apoptosis rate of 17.30±3.46%, both OG-HMPs@BMSCs and G-HMPs@BMSCs significantly reduced OGC apoptosis rates (7.64 ± 0.85% and 8.72 ± 1.24%, respectively), with no significant difference between these two groups (Figures 3D-E). The endocrine function of OGCs was assessed by measuring hormone levels in cell culture supernatants via ELISA. The OG-HMPs@BMSCs group showed significantly higher secretion levels of E2 and AMH compared to control groups (Figure 3F). These results indicate that OG-HMPs@BMSCs not only promote the survival of damaged OGCs but also enhance their hormone secretion function.

OG-HMPs@BMSCs augment BMSCs retention and therapeutic efficacy in POI model

Female C57BL/6 mice aged 8–10 weeks and weighing 20–25 g were selected for this study. A chemically induced POI mouse model was established. Adult female C57BL/6 model mice were intraperitoneally injected with cyclophosphamide at a dose of 40 mg/kg per day for 8 days, and then with cyclophosphamide at a dose of 20 mg/kg per day for 7 consecutive days. The mice in the control group were injected with normal saline. Serum analysis revealed that, compared with normal mice, POI model mice presented elevated FSH levels and decreased AMH and E2 levels (Figure S10A). Furthermore, ovaries from POI model mice presented a greater number of atretic follicles and a significantly reduced number of growing follicles, confirming the successful establishment of the POI mouse model

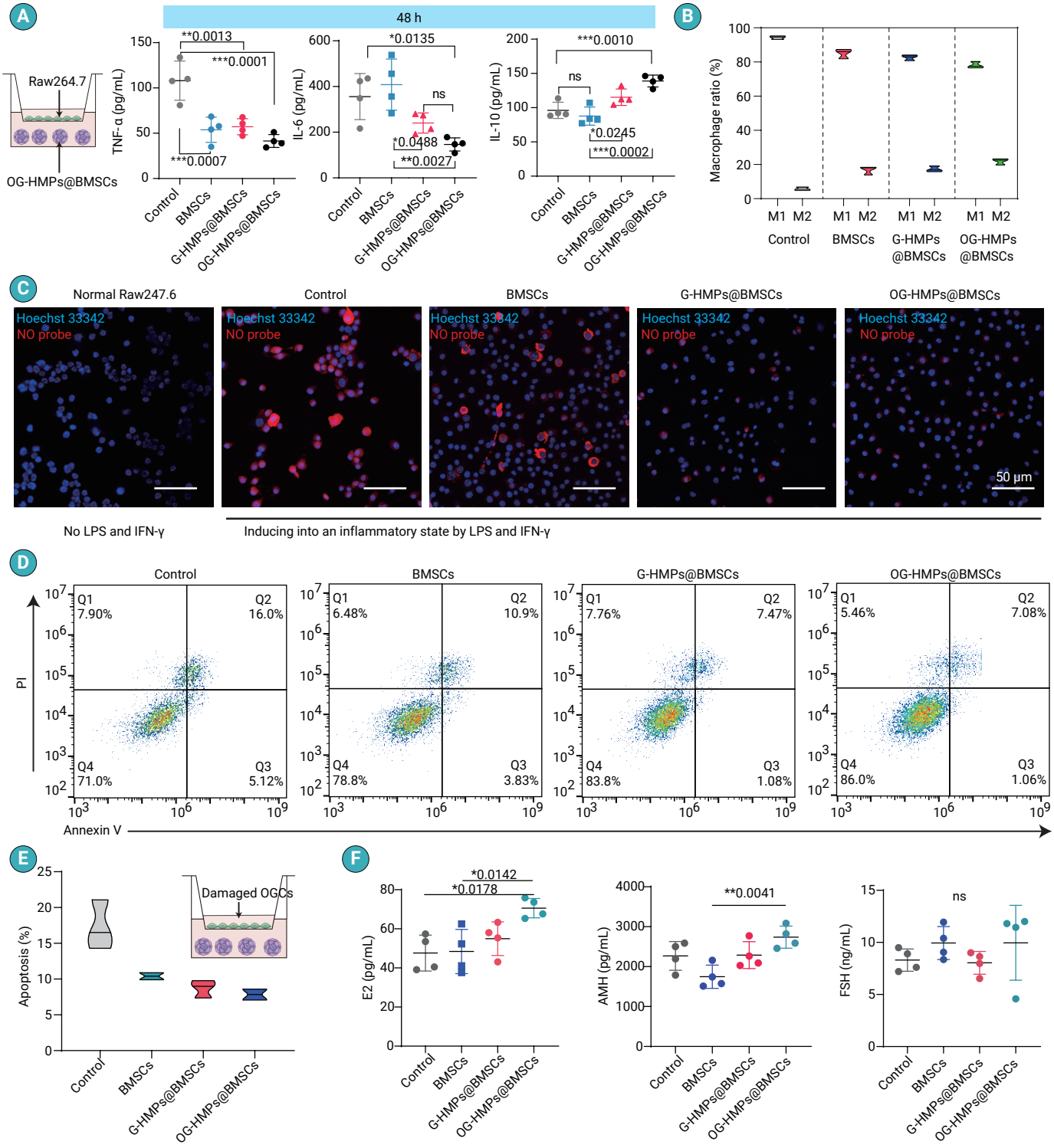

Figure 3. OG-HMPs@BMSCs-mediated immunomodulation and cytoprotection of OGCs (A) ELISA measurement of proinflammatory (TNF-α, IL-6) and anti-inflammatory (IL-10) cytokine secretion levels in the culture supernatant of macrophages that stimulated with LPS (200 ng/mL) and IFN-γ (2.5 ng/mL) for 12 hours. The data are presented as the means ± SDs (n = 4). Statistical analysis was performed using one-way ANOVA followed by GraphPad Prism 8.0.2. * $p < 0.05$, ** $p < 0.01$. (B) Flow cytometric analysis of macrophage polarization. The data are presented as percentages of M1 ($F4/80^+$ $CD11b^+$ $iNOS^+$) and M2 ($F4/80^+$ $CD11b^+$ Arg^+) macrophages. The bar graph shows the M2/M1 ratios of the different treatment groups. (C) Fluorescence microscopy images showing NO probe expression (red fluorescence) in macrophages under different treatment conditions. Nuclei were stained with DAPI (blue). Scale bar: 50 μm. (D-E) Representative flow cytometry scatter plots showing the Annexin V/PI staining results and statistical information for OGCs after different treatments. (F) ELISA detection of E2, FSH, and AMH levels in OGCs culture supernatants. Data are presented as means ± SD (n = 4). Statistical analysis was performed using one-way ANOVA followed by Tukey's post hoc test (GraphPad Prism 8.0.2). * $p < 0.05$, ** $p < 0.01$.

(Figures S10B-C).

POI model mice were randomly assigned to three groups (n = 12): the untreated POI group (injected with 50 μL of saline), the BMSCs group (injected with 50 μL of a cell suspension containing 6×10^5 mouse BMSCs, the OG-HMPs@BMSCs group (injected with 50 μL of OG-HMPs loaded with $6{\times}10^5$ BMSCs) (Figure 4A). Additionally, a Normal group (n = 10, healthy mice without treatment) was set as a positive control. To monitor the *in vivo* retention and distribution of the transplanted BMSCs, the cells were labeled with DiD before injection (Figures S11A-B). *In vivo* fluorescence imaging revealed that OG-HMPs@BMSCs substantially enhanced the retention of transplanted

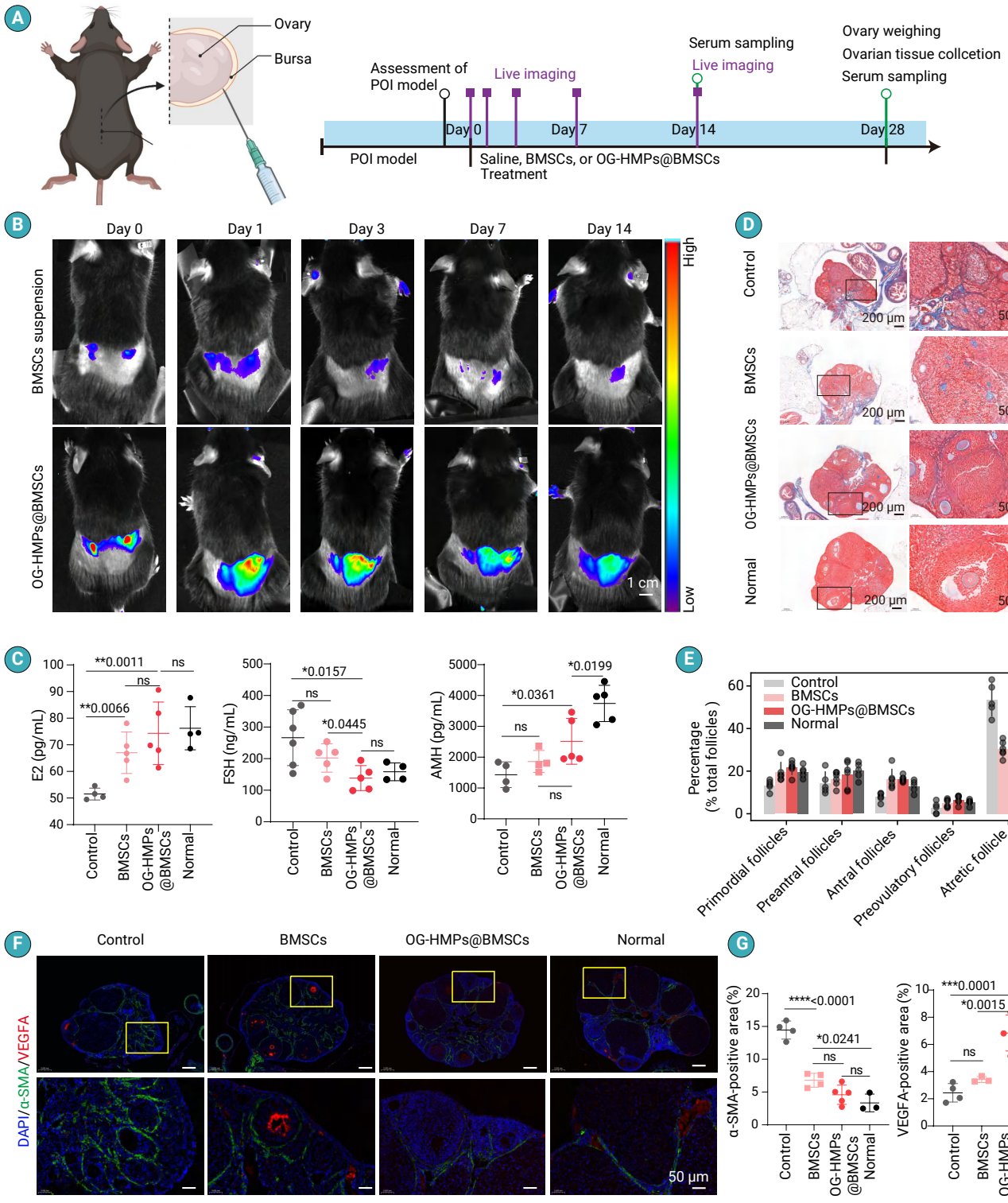

Figure 4. OG-HMPs delivering BMSCs for POI treatment in mice (A) Timeline of *in vivo* experimental design. (Created in BioRender. Liu, X. (2025) https://BioRender.com/e74y943.) POI mouse model was established, followed by treatment with saline, BMSCs, or OG-HMPs@BMSCs. Multiple assessment time points including live imaging (Day 0, 1, 3, 7, 14) and serum sampling (Day 14, 28) were conducted. Final ovary weighing and ovarian tissue collection were performed on Day 28. (B) *In vivo* fluorescence imaging showing the distribution of DiD-labeled BMSCs at 0, 1, 3, 7, and 14 days after transplantation. (C) Serum E2, FSH, and AMH levels in POI mice measured by ELISA at day 28 post-treatment (n ≥ 4). The data are presented as the means ± SDs. Statistical analysis was performed using one-way analysis of variance (ANOVA) followed by Tukey's multiple comparison test. * $p < 0.05$, ** $p < 0.01$. (D) Masson staining of ovarian tissue. Left scale bar: 200 μm; right row scale bar: 50 μm. (E) Quantification of follicle distribution in ovarian tissues across different treatment groups. Bar graphs show the percentages of primordial, preantral, antral, preovulatory, and atretic follicles in different groups (n≥5). (F) Immunofluorescence staining showing the expression of a fibrosis marker (α-SMA, green) and an angiogenesis marker (VEGFA, red) in ovarian tissue. Nuclei were stained with DAPI (blue). Scale bar: 200 μm. (G) Statistical analysis of the α-SMA immunofluorescence-positive area. The data are presented as the means ± SDs (n≥3). Statistical analysis was performed using one-way analysis of variance (ANOVA) followed by Tukey's multiple comparison test. * $p < 0.05$, ** $p < 0.01$, *** $p < 0.001$, **** $p < 0.0001$.

stem cells within ovarian tissues. Strong fluorescent signals remained detectable in the OG-HMPs@BMSCs group on day 14 posttransplantation, whereas the directly injected BMSCs presented minimal retention with rapidly diminishing signals by day 3 (Figure 4B). To evaluate the therapeutic effects of the different treatments, the mice were euthanized on day 28, and the ovarian index (ovary wet weight/body weight ratio) was calculated to assess ovarian health (Figure S11C). The ovarian index was significantly lower in the untreated POI group (0.0528 ± 0.0045%) than in the normal group (0.0658 ± 0.0032%), confirming the successful establishment of chemotherapy-induced ovarian dysfunction. Compared with untreated POI group, both the BMSCs group (0.06247 ± 0.0031%) and the OG-HMPs@BMSCs group (0.0674 ± 0.0041%) presented significantly increased ovarian indices. Serum levels of E2, FSH, and AMH were measured via ELISA at days 14 and 28 posttreatment to assess ovarian function (Figures S11D & S4C). Compared with no treatment (Control), OG-HMPs@BMSCs treatment significantly increased E2 and AMH levels while decreasing FSH levels in POI model mice. Notably, the E2 levels in the OG-HMPs@BMSCs group were restored to levels comparable to those in the normal controls. Although direct BMSCs injection also altered the hormonal profile, the therapeutic effect was less robust than that of OG-HMPs@BMSCs treatment (Figures S11D & S4C). These findings demonstrate that OG-HMPs@BMSCs effectively restore ovarian endocrine function in POI model mice.

Masson staining analysis of ovarian tissue revealed that the ovaries of untreated POI model mice presented severe tissue atrophy with marked follicular depletion, particularly depletion of growing and mature follicles, accompanied by increased interstitial fibrosis (blue staining) as a feature of POI pathology (Figure 4D). BMSCs transplantation partially restored ovarian morphology, as evidenced by the presence of primordial and some growing follicles, although mature follicles remained scarce and interstitial fibrosis persisted. In contrast, OG-HMPs@BMSCs treatment demonstrated superior therapeutic efficacy, with follicles observed across all developmental stages and reduced fibrosis, closely resembling normal ovarian architecture. Follicle counting was performed on Masson-stained sections from the largest cross-sectional area of ovaries. Follicles were classified into six categories: primordial follicles, preantral follicles, antral follicles, preovulatory follicles, corpora lutea, and atretic follicles (Figure S12A). Follicle counting analysis revealed that the total number of follicles in the OG-HMPs@BMSCs group (34.8 ± 2.2) was significantly higher than that in both control and BMSCs groups, approaching the level of the normal group (Figures 4E & S12B). The numbers and proportions of primordial and preantral follicles in the OG-HMPs@BMSCs group were significantly higher than those in the control group. Growing follicles, including antral and preovulatory follicles, showed slightly higher numbers compared to the BMSCs group and were markedly increased compared to the control group. Additionally, the proportion of atretic follicles in the OG-HMPs@BMSCs group was significantly reduced compared to the control group (53.6 ± 7.7%), reaching levels similar to the normal group (Figure 4E). These results demonstrate that OG-HMPs@BMSCs treatment effectively maintains follicular reserve, promote follicular development, and significantly inhibit pathological follicular atresia, resulting in follicular development patterns more closely resembling normal physiological conditions.

We then performed immunofluorescence staining to examine the expression of α-smooth muscle actin (α-SMA) and vascular endothelial growth factor (VEGF) in ovarian sections (Figure 4F). The untreated POI ovaries showed extensive α-SMA immunoreactivity, indicating severe fibrosis. OG-HMPs@BMSCs treatment reduced α-SMA expression to levels similar to those in the normal group. Quantitative analysis showed that the α-SMA-positive area in the OG-HMPs@BMSCs group decreased by approximately 10% compared to Control group (Figure 4G). Compared to the Control group, both BMSCs-only and OG-HMP@BMSCs groups exhibited significantly elevated VEGFA expression, with the OG-HMP@BMSCs group approaching levels observed in normal group (Figure 4G). These findings suggest that OG-HMP@BMSCs therapy not only reduces pathological fibrosis but also promotes angiogenesis, potentially creating a more favorable microenvironment for ovarian follicle development and functional recovery in POI.

Molecular characterization of OG-HMPs@BMSCs-mediated ovarian regeneration

Immunofluorescence staining was conducted to assess ovarian reserve and stromal remodeling. As illustrated in Figure 5A, immunofluorescence analysis of ovarian sections demonstrated differential expression of ovarian markers across treatment groups. Both BMSCs and OG-HMPs@BMSCs groups exhibited elevated expression of the ovarian reserve marker AMH and the ovarian function marker follicle-stimulating hormone receptor (FSHR) compared to the control group. Further analysis revealed that AMH expression was significantly higher in both OG-HMPs@BMSCs and Normal groups compared to the control group, though no significant difference was observed between OG-HMPs@BMSCs and BMSCs groups (Figure 5C). FSHR expression, however, showed significant increases in both OG-HMPs@BMSCs and Normal groups when compared specifically to the BMSCs group (Figure 5D). To investigate the functional impact of these treatments, we examined proliferation and follicular development markers, which revealed increasing expression of Ki67 and INHBA in the OG-HMPs@BMSCs group compared to Control and BMSCs groups (Figure 5B). The elevated Ki67 expression indicated enhanced cellular proliferation in treated ovarian tissue,[40,41] particularly in granulosa cells which are essential for follicular development and hormone production. Quantitative analysis of fluorescence intensity confirmed that Ki67 and INHBA expression in the OG-HMPs@BMSCs group surpassed both control and BMSCs groups, reaching levels similar to normal controls (Figures 5E-F). The increased INHBA, a key component of the activin-inhibin system, suggested improved follicular development and granulosa cell function.[42] This INHBA enhanced expression pattern implies the restoration of normal folliculogenesis regulatory networks.

Regarding cell apoptosis, immunohistochemical staining revealed prominent Caspase 3 immunoreactivity in the control group. While BMSCs transplantation partially suppressed Caspase 3 expression, the OG-HMPs@BMSCs treatment group demonstrated minimal apoptotic signals, accompanied by organized cellular arrangement and increased cellular density, with improved tissue organization and cellular density (Figure 5G). The positive staining area of Caspase-3 (pro-apoptotic) in the OG-HMPs@BMSCs group was significantly lower than that in other groups (Figure 5H). PCR analysis confirmed these findings, showing increased Bcl-2 (anti-apoptotic), decreased Caspase 3, and maintained AMH expression in the OG-HMPs@BMSCs group (Figure 5I). This molecular signature suggests that our therapeutic approach effectively modulates the balance between pro-survival and pro-apoptotic pathways, creating an environment conducive to follicular survival and development.

Therapeutic efficacy of OG-HMPs@BMSCs on reproductive function restoration

We evaluated the estrous cycling pattern through continuous 14-day vaginal cytological examination (Figure 6A). The normal estrous cycle in mice, comprising proestrus, estrus, metestrus, and diestrus phases, exhibited distinctive patterns reflecting ovarian function across different treatment groups (Figures 6B-C). Mice in the POI group predominantly remained in diestrus, accounting for 67.1% of the observation period, indicating compromised ovarian function (Figure 6D). This phenomenon corresponds with clinical manifestations in POI patients, including amenorrhea and hormonal abnormalities. In contrast, the normal group displayed the typical 4-5 day cyclic pattern with orderly transitions between proestrus, estrus, metestrus, and diestrus phases (Figures 6B & S13). The BMSCs treatment group demonstrated partially restored estrous cycling, although diestrus still predominated (55.7%), suggesting that BMSCs therapy confers moderate repair effects on ovarian function (Figure 6D). Mice in the OG-HMPs@BMSCs treatment group exhibited more regular estrous cycling patterns, with diestrus proportion decreasing to 40.0% and estrus frequency significantly increasing, approaching the normal group's diestrus level of 34.3% (Figure 6D). We further quantified the average estrous cycle length across groups. The POI group displayed markedly prolonged cycles (7.8 ± 1.2 days), while the normal group maintained typical cycles of 4.3 ± 0.5 days. BMSCs treatment shortened the cycle to 6.0±0.8 days, while OG-HMPs@BMSCs treatment further reduced it to 5.3 ± 0.7 days (Figure 6E). This improvement in estrous cyclicity likely correlates with the previously observed restoration of

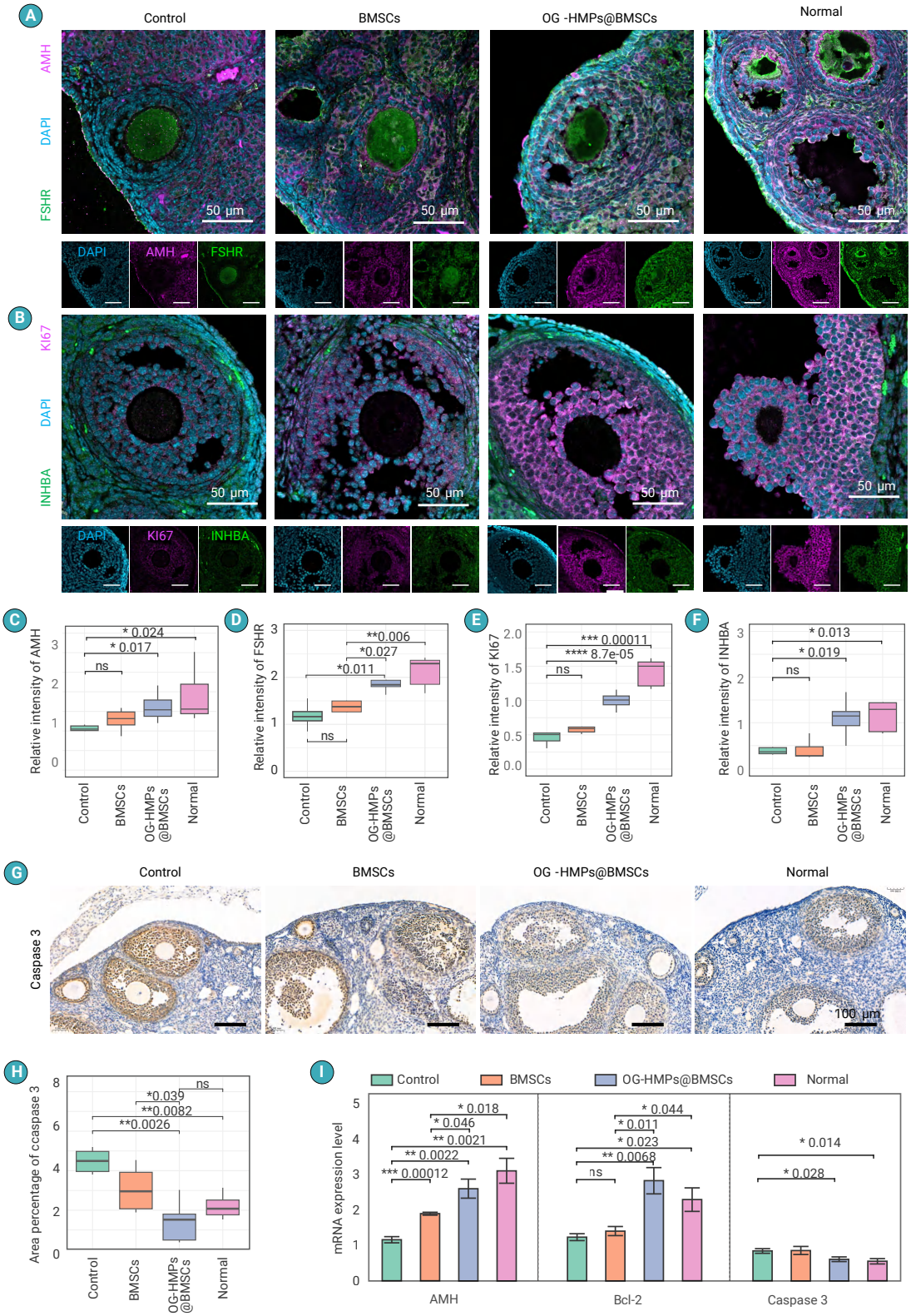

Figure 5. Immunofluorescence and histological analysis of ovarian tissue (A) Representative immunofluorescence images of ovarian tissue sections from different treatment groups (control, BMSCs, OG-HMPs@BMSCs, and normal groups). Sections were stained for DAPI (blue, nuclei), AMH (magenta, an ovarian reserve marker), and FSHR (green, an ovarian function marker). Scale bar: 50 μm. (B) Immunofluorescence staining of ovarian tissue sections showing the expression of DAPI (blue, nuclei), Ki67 (magenta, proliferation marker), and INHBA (green, follicular development marker). Scale bar: 50 μm. (C-F) Quantitative analysis of the relative fluorescence intensities of AMH, FSHR, Ki67, and INHBA in ovarian tissue from different treatment groups. The nuclear mean fluorescence intensity (MFI) serving as an internal normalization factor to account for cell density variations. Marker protein MFI / nuclear MFI was the formula used to determine the relative fluorescence intensity. The data are presented as the means ± SDs. Statistical analysis was performed using Student's t-test in R package v.4.4.2. * $p < 0.05$, ** $p < 0.01$, *** $p < 0.001$. (G) Immunohistochemical staining for Caspase 3 in ovarian tissue from different treatment groups. Scale bar: 50 μm. (H) Immunohistochemical staining for Caspase 3 in ovarian tissue from different treatment groups. Scale bar: 50 μm. (I) Relative mRNA expression levels, including those of Bcl-2, AMH, and Caspase 3, in ovarian tissues from different experimental groups (n = 3). The data are presented as the means ± SDs. Statistical analysis was performed using Student's t-test in R package v.4.4.2. * $p < 0.05$, ** $p < 0.01$.

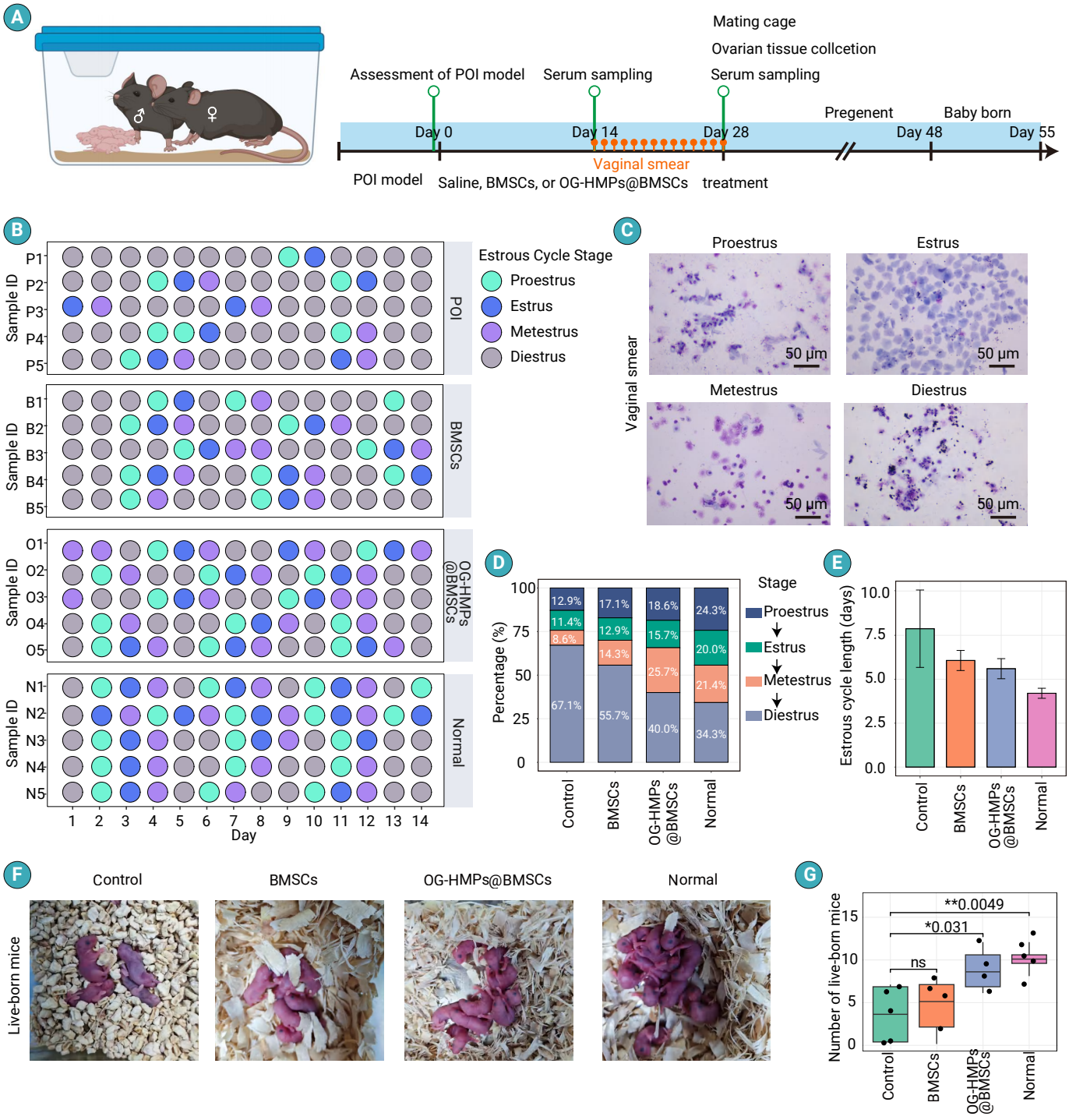

Figure 6. Assessment of ovarian function and fertility (A) Experimental timeline schematic. Created in BioRender. Liu, X. (2025) https://BioRender.com/e74y943. (B) Visual representation of estrous cycle patterns in mice from different experimental groups over a 14-day monitoring period. Each row represents an individual mouse. (C) Giemsa-stained mouse vaginal smear images. Representative microscopy images showing the proestrus, estrus, metestrus, and diestrus phases. Scale bar: 50 μm. (D) Percentage distribution of estrous cycle stages across different experimental groups during the monitoring period. (E) Statistical analysis of the number of complete estrous cycles in mice from different experimental groups during the 14-day monitoring period. (F) Representative photographs of live-born pups from the cohousing mating experiment conducted 21 days after treatment. (G) Statistical analysis of the number of live-born pups from different experimental groups. The data are presented as the means ± SDs (n ≥ 4). Data are presented as mean ± SDs. Statistical significance was determined by unpaired Student's t-test. * $p < 0.05$, ** $p < 0.01$, *** $p < 0.001$.

ovarian reserve (upregulated AMH expression) and optimization of the follicular development microenvironment (increased INHBA expression).

To further assess reproductive function, we conducted fertility assessment 28 days post-treatment. Two female mice from each group were paired with male mice for one week (Figure 6F). Statistical analysis at 20 days post-mating showed that the OG-HMPs@BMSCs group achieved a 100% parturition rate comparable to the normal group, with significantly higher litter size compared to both POI control and BMSCs groups (Figure 6G). This result is mutually corroborated with the improvement observed in estrous cycles, supporting that OG-HMPs@BMSCs treatment can significantly restore reproductive function in POI mice. The improvement in fertility likely stems from the previously demonstrated dual mechanisms: inhibition of aberrant cell

apoptosis through the Bcl-2/Caspase 3 pathway, maintaining ovarian cell viability; and enhancement of cell proliferation through Ki67 expression, optimizing the follicular development microenvironment, ultimately achieving comprehensive restoration of ovarian function.

In conclusion, these data demonstrate that OG-HMPs@BMSCs treatment effectively restores ovarian function in the POI mouse model, resulting in both normalized estrous cycling patterns and enhanced reproductive capacity. This therapeutic approach provides novel mechanistic insights and experimental evidence for the potential treatment of POI patients.

CONCLUSIONS

In tissue engineering approaches, the development of scaffolds or hydrogels mimicking the ovarian extracellular matrix (ECM) constitutes a pivotal strategy to support follicular survival and development. Previous studies have validated that ovarian ECM-derived hydrogels fabricated from decellularized ovarian matrices can effectively sustain three-dimensional follicular cultures in vitro.[42] Within regenerative medicine paradigms, MSCs transplantation demonstrates therapeutic potential for ovarian functional restoration through multifaceted mechanisms, including folliculogenesis promotion, hormonal homeostasis modulation, and granulosa cell apoptosis suppression.[13,14] Nevertheless, clinical translation remains constrained by technical limitations such as suboptimal cellular retention rates, transient survival kinetics, and oncogenic safety concerns.[15]

To overcome these translational barriers, our study introduces an innovative OG-HMPs system employing functionalized biomaterials as stem cell carriers. This platform demonstrates significant advancements over conventional direct injection protocols by substantially enhancing the spatial localization efficiency and prolonged retention capacity of BMSCs within ovarian tissue. The OG-HMPs@BMSCs system demonstrated significant efficacy in restoring ovarian function via multifaceted mechanisms. At the molecular level, the treatment upregulated anti-apoptotic marker and ovarian reserve marker AMH while downregulating pro-apoptotic Caspase-3. Furthermore, OG-HMPs@BMSCs exhibited immunomodulatory effects by promoting M2 macrophage polarization and suppressing pro-inflammatory cytokine secretion, thereby fostering a regenerative microenvironment conducive to ovarian tissue repair. Notably, the OG-HMPs@BMSCs group showed enhanced outcomes in follicle count, fertility restoration, and estrous cycle normalization compare to direct cell injection. OG-HMPs supported sustained BMSCs functionality and more stable therapeutic outcomes, highlighting their advantages for long-term efficacy and clinical translatability. This study primarily examines the augmented therapeutic potential of BMSCs facilitated by OECM, however the possible direct role of OECM components in ovarian tissue repair cannot be completely dismissed. We recognize that through processes like protein-protein interactions, the addition of tissue-specific extracellular matrix components seems to support tissue regeneration and repair.[44,45]

In conclusion, this study provides robust experimental evidence supporting OG-HMPs@BMSCs delivery system as a promising therapeutic strategy for POI. By integrating molecular, cellular, endocrine, and functional recovery mechanisms, this biomaterial-engineered approach significantly improved ovarian function and reproductive outcomes. Our findings emphasize the transformative potential of biomaterial-enhanced stem cell delivery systems in ovarian regeneration. Future research should prioritize long-term therapeutic durability assessments, optimization of clinical translation parameters, and comprehensive safety evaluations to advance this innovative strategy toward clinical application. Also, stem cell-derived exosomes mediate paracrine regenerative effects through sophisticated cargo delivery systems containing proteins, mRNAs, and microRNAs, establishing a novel cell-free therapeutic paradigm for ovarian rejuvenation. While this strategy circumvents risks associated with whole-cell transplantation, its therapeutic durability may be inferior to bioengineered living cell systems encapsulated within functional matrices that enable dynamic microenvironmental regulation.

REFERENCES

1. De Vos M., Devroey P. and Fauser B.C. (2010). Primary ovarian insufficiency. *Lancet* **376**:911–921. DOI:10.1016/S0140-6736(10)60355-8
2. Falsetti L., Scalchi S., Villani M.T., et al. (1999). Premature ovarian failure. *Gynecol. Endocrinol.* **13**:189–195. DOI:10.3109/09513599909167554
3. Cao C., Pei W., Zhou P., et al., (2024). GNAS deficiency is associated with premature ovarian insufficiency phenotype via regulating ovarian steroidogenesis. *The Innovation Life* **2**: 100080. DOI:10.59717/j.xinn-life.2024.100080
4. Chernyshov V.P., Radysh T.V., Gura I.V., et al. (2001). Immune Disorders in Women with Premature Ovarian Failure in Initial Period. *Am. J. Reprod. Immunol.* **46**:220–5. DOI:10.1034/j.1600-0897.2001.d01-5.x
5. Deng T., He J., Yao Q., et al. (2021). Human Umbilical Cord Mesenchymal Stem Cells Improve Ovarian Function in Chemotherapy-Induced Premature Ovarian Failure Mice Through Inhibiting Apoptosis and Inflammation via a Paracrine Mechanism. *Reprod. Sci.* **28**:1718–32. DOI:10.1007/s43032-021-00499-1
6. Kapoor E. (2023). Premature Ovarian Insufficiency. *Curr. Opin. Endocr. Metab. Res.* **28**:100435. DOI:10.1016/j.coemr.2023.100435
7. Zhang S., Zhu D., Li Z., et al. (2021). A stem cell-derived ovarian regenerative patch restores ovarian function and rescues fertility in rats with primary ovarian insufficiency. *Theranostics* **11**:8894–908. DOI:10.7150/thno.61690
8. Takahashi A., Yousif A., Hong L., et al. (2021). Premature ovarian insufficiency: pathogenesis and therapeutic potential of mesenchymal stem cell. *J. Mol. Med.* **99**:637–50. DOI:10.1007/s00109-021-02055-5
9. Na J. and Kim G.J. (2020). Recent trends in stem cell therapy for premature ovarian insufficiency and its therapeutic potential: a review. *J. Ovarian Res.* **13**:74. DOI:10.1186/s13048-020-00671-2
10. Wang J., Liu W., Yu D., et al. (2021). Research Progress on the Treatment of Premature Ovarian Failure Using Mesenchymal Stem Cells: A Literature Review. *Front. Cell Dev. Biol.* **9**:749822. DOI:10.3389/fcell.2021.749822
11. Sun B., Ma Y., Wang F., et al. (2019). miR-644-5p carried by bone mesenchymal stem cell-derived exosomes targets regulation of p53 to inhibit ovarian granulosa cell apoptosis. *Stem Cell Res. Ther.* **10**:360. DOI:10.1186/s13287-019-1442-3
12. Ran X., Wang Q., Sun Y., et al. (2024). Dual microparticles programmed delivery system regulating stem cell-based cartilage regeneration by cartilage-specific matrix hydrogels. *Compos. Part B: Eng.* **272**:111221. DOI:10.1016/j.compositesb.2024.111221
13. Fu X., He Y., Xie C., et al. (2008). Bone marrow mesenchymal stem cell transplantation improves ovarian function and structure in rats with chemotherapy-induced ovarian damage. *Cytotherapy* **10**:353–363. DOI:10.1080/14653240802035926
14. N K., Hr S., M M., et al. (2018). Effect of transplantation of bone marrow stromal cell-conditioned medium on ovarian function, morphology and cell death in cyclophosphamide-treated rats. *Cell J.* **20**:10–18. DOI:10.22074/cellj.2018.4919
15. Fischer U.M., Harting M.T., Jimenez F., et al. (2009). Pulmonary passage is a major obstacle for intravenous stem cell delivery: the pulmonary first-pass effect. *Stem Cells Dev.* **18**:683–691. DOI:10.1089/scd.2008.0253
16. Wang L., Mei Q., Xie Q., et al. (2022). A comparative study of mesenchymal stem cells transplantation approach to antagonize age-associated ovarian hypofunction with consideration of safety and efficiency. *J. Adv. Res.* **38**:245–259. DOI:10.1016/j.jare.2021.09.001
17. Laronda M.M., Rutz A.L., Xiao S., et al. (2017). A bioprosthetic ovary created using 3D printed microporous scaffolds restores ovarian function in sterilized mice. *Nat. Commun.* **8**:1–10. DOI:10.1038/ncomms15261
18. Taraballi F., Sushnitha M., Tsao C., et al. (2018). Biomimetic tissue engineering: tuning the immune and inflammatory response to implantable biomaterials. *Adv. Healthc. Mater.* **7**:1800490. DOI:10.1002/adhm.201800490
19. Que R., Mohraz A., Da Silva N.A., et al. (2014). Expanding functionality of recombinant human collagen through engineered non-native cysteines. *Biomacromolecules* **15**:3540–3549. DOI:10.1021/bm500735d
20. Chen Y., Chen L.-F., Wang Y., et al. (2025). Engineered dECM-based microsystem promotes cartilage regeneration in osteoarthritis by synergistically enhancing chondrogenesis of BMSCs and anti-inflammatory effect. *Compos. Part B: Eng.* **290**:111974. DOI:10.1016/j.compositesb.2024.111974
21. Yuan X., Wei Y., Villasante A., et al. (2017). Stem cell delivery in tissue-specific hydrogel enabled meniscal repair in an orthotopic rat model. *Biomaterials* **132**:59–71. DOI:10.1016/j.biomaterials.2017.04.004
22. Rao N., Agmon G., Tierney M.T., et al. (2017). Engineering an injectable muscle-specific microenvironment for improved cell delivery using a nanofibrous extracellular matrix hydrogel. *ACS Nano* **11**:3851–3859. DOI:10.1021/acsnano.7b00093
23. Wu T., Huang K.-C., Yan J.-F., et al. (2023). Extracellular matrix-derived scaffolds in constructing artificial ovaries for ovarian failure: a systematic methodological review. *Hum. Reprod. Open* **2023**:hoad014. DOI:10.1093/hropen/hoad014
24. Zhao Z., Wang Z., Li G., et al. (2021). Injectable microfluidic hydrogel microspheres for cell and drug delivery. *Adv. Funct. Mater.* **2103339**:1–24. DOI:10.1002/adfm.202103339
25. Wang S., Wang Z., Shen Z., et al. (2024). Magnetic soft microrobots for erectile dysfunction therapy. *Proc. Natl. Acad. Sci. USA* **121**:e2407809121. DOI:10.1073/pnas.2407809121
26. An G., Guo F., Liu X., et al. (2020). Functional reconstruction of injured corpus cavernosa using 3D-printed hydrogel scaffolds seeded with HIF-1α-expressing stem cells. *Nat. Commun.* **11**:2687. DOI:10.1038/s41467-020-16192-x
27. Francés-Herrero E., Lopez R., Campo H., et al. (2023). Advances of xenogeneic

ovarian extracellular matrix hydrogels for *in vitro* follicle development and oocyte maturation. *Biomater. Adv.* **151**:213480. DOI:10.1016/j.bioadv.2023.213480
28. Li Y., Zhang H., Cai C., et al. (2024). Microfluidic encapsulation of exosomes derived from lipopolysaccharide-treated mesenchymal stem cells in hyaluronic acid methacryloyl to restore ovarian function in mice. *Adv. Healthc. Mater.* **13**:2303068. DOI:10.1002/adhm.202303068
29. Liu X., Chen Y., Mao A.S., et al. (2020). Molecular recognition-directed site-specific release of stem cell differentiation inducers for enhanced joint repair. *Biomaterials* **232**:119644. DOI:10.1016/j.biomaterials.2019.119644
30. Wang Z., An G., Zhu Y., et al. (2019). 3D-printable self-healing and mechanically reinforced hydrogels with host-guest non-covalent interactions integrated into covalently linked networks. *Mater. Horiz.* **6**:733–742. DOI:10.1039/c8mh01208c
31. Zhang W., Chen J., Tao J., et al. (2013). The use of type 1 collagen scaffold containing stromal cell-derived factor-1 to create a matrix environment conducive to partial-thickness cartilage defects repair. *Biomaterials* **34**:713–723. DOI:10.1016/j.biomaterials.2012.10.027
32. Kulus J., Kulus M., Kranc W., et al. (2021). Transcriptomic profile of new gene markers encoding proteins responsible for structure of porcine ovarian granulosa cells. *Biology (Basel)* **10**:1214. DOI:10.3390/biology10111214
33. Mantri M., Zhang H.H., Spanos E., et al. (2024). A spatiotemporal molecular atlas of the ovulating mouse ovary. *Proc. Natl. Acad. Sci. USA* **121**:e2317418121. DOI:10.1073/pnas.2317418121
34. Crapo P.M., Gilbert T.W., Badylak S.F. (2011). An overview of tissue and whole organ decellularization processes. *Biomaterials* **32**:3233–3243. DOI:10.1016/j.biomaterials.2011.01.057
35. Kennelly H., Mahon B.P., English K. (2016). Human mesenchymal stromal cells exert HGF dependent cytoprotective effects in a human relevant pre-clinical model of COPD. *Sci. Rep.* **6**:38207. DOI:10.1038/srep38207
36. Chang H.-K., Kim P.-H., Kim D.W., et al. (2018). Coronary stents with inducible VEGF/HGF-secreting UCB-MSCs reduced restenosis and increased re-endothelialization in a swine model. *Exp. Mol. Med.* **50**:1–14. DOI:10.1038/s12276-018-0143-9
37. Chi A., Yang B., Dai H., et al. (2024). Stem Leydig cells support macrophage immunological homeostasis through mitochondrial transfer in mice. *Nat. Commun.* **15**:2120. DOI:10.1038/s41467-024-46190-2
38. Saraiva M. and O'Garra A. (2010). The regulation of IL-10 production by immune cells. *Nat. Rev. Immunol.* **10**:170–181. DOI:10.1038/nri2711
39. Huang Y., Zhu M., Liu Z., et al. (2022). Bone marrow mesenchymal stem cells in premature ovarian failure: mechanisms and prospects. *Front. Immunol.* **13**:997808. DOI:10.3389/fimmu.2022.997808
40. Ding C., Zou Q., Wang F., et al. (2018). Human amniotic mesenchymal stem cells improve ovarian function in natural aging through secreting hepatocyte growth factor and epidermal growth factor. *Stem Cell Res. Ther.* **9**:55. DOI:10.1186/s13287-018-0781-9
41. Zhou Y., Zhou J., Xu X., et al. (2021). Matrigel/umbilical cord-derived mesenchymal stem cells promote granulosa cell proliferation and ovarian vascularization in a mouse model of premature ovarian failure. *Stem Cells Dev.* **30**:782–796. DOI:10.1089/scd.2021.0005
42. Ma M., Wang H., Zhang Y., et al. (2021). circRNA-mediated inhibin–activin balance regulation in ovarian granulosa cell apoptosis and follicular atresia. *Int. J. Mol. Sci.* **22**:9113. DOI:10.3390/ijms22179113
43. Chiti M.-C., Vanacker J., Ouni E., et al. (2022). Ovarian extracellular matrix-based hydrogel for human ovarian follicle survival in vivo: a pilot work. *J. Biomed. Mater. Res. B* **110**:1012–1022. DOI:10.1002/jbm.b.34974
44. Yi X., Liu F., Gao K., et al. (2022). Reconstructable uterus - derived materials for uterus recovery toward efficient live births. *Adv. Mater.* **34**:2106510. DOI:10.1002/adma.202106510
45. Chiti M.-C., Vanacker J., Ouni E., et al. (2022). Ovarian extracellular matrix - based hydrogel for human ovarian follicle survival in vivo: a pilot work. *J. Biomed. Mater. Res. B* **110**:1012–1022. DOI:10.1002/jbm.b.34974

FUNDING AND ACKNOWLEDGMENTS

This work was financially supported by the National Natural Science Foundation of China (32301136, U22A20157), the China Postdoctoral Science Foundation (2024M760642), the Guangdong Basic and Applied Basic Research Foundation (2022B1515130010). The funders had no role in study design, data collection and analysis, decision to publish or preparation of the manuscript.

AUTHOR CONTRIBUTIONS

Xuemin Liu: Conceptualization, Data curation, Formal analysis, Funding acquisition, Investigation, Methodology, Software, Validation, Visualization, Writing – original draft. Ming Chen: Investigation, Data curation, Formal analysis, Visualization. Xiaojie Liang: Methodology, Software, Validation. Peixian Liang: Investigation, Data curation, Methodology. Zeshen Liang: Data curation, Investigation. Yong Fan: Conceptualization, Methodology, Supervision, Writing - review & editing, Project administration, Funding acquisition. Xuetao Shi: Funding acquisition, Project administration, Supervision, Writing – review & editing. All authors contributed to the manuscript and approved the final version.

DECLARATION OF INTERESTS

Xuetao Shi is an Editorial Board member of The Innovation Life and was blinded from reviewing or making final decisions on the manuscript. Peer review was handled independently of this member and their research group. The other authors declare no conflicts of interest.

ETHICAL STATEMENT AND PATIENT CONSENT

The study was approved by the ethics committee of South China University of Technology and Guangzhou Shuiyuntian Biotechnology Co. , Ltd. (SYT2024069) and was conducted in accordance with the Declaration of Helsinki.

DATA AND CODE AVAILABILITY

Data generated or analyzed during this study are included in the published article and its Supplemental information. Any additional data are available from the corresponding author upon reasonable request.

SUPPLEMENTAL INFORMATION

It can be found online at https://doi.org/10.59717/j.xinn-life.2025.100147